Inorg. Chem. **2002**, *41*, 4461–4467

Site Specificity of Metal Ions in Heterodinuclear Complexes Derived from an "End-Off" Compartmental Ligand

Koji Abe, Kanako Matsufuji, Masaaki Ohba,* and Hisashi Ōkawa*

Department of Chemistry, Faculty of Science, Kyushu University, Hakozaki 6-10-1, Higashiku, Fukuoka 812-8581, Japan

Received January 2, 2002

A phenol-based "end-off" compartmental ligand, 2-{*N*-[2-(dimethylamino)ethyl]iminomethyl}-6-[*N*,*N*-di(2-pyridylmethyl)-aminomethyl]-4-methylphenol (HL), having a bidentate arm and a tridentate arm attached to the 2 and 6 positions of the phenolic ring, has afforded the following heterodinuclear $M_a^{II}M_b^{II}$ complexes: $[CuM(L)(AcO)_2]ClO_4$ (M = Mn (**1**), Fe (**2**), Co (**3**), Ni (**4**), Zn (**5**)), $[ZnM(L)(AcO)_2]ClO_4$ (M = Co (**6**), Ni (**7**)), and $[CuNi(L)(AcO)(NCS)_2]$ (**8**). **1**·MeOH (**1′**), **2**·MeOH (**2′**), **3**·MeOH (**3′**), **4**·MeOH (**4′**), **5**·MeOH (**5′**), and **7**·MeOH (**7′**) are isostructural and have a heterodinuclear core bridged by the phenolic oxygen atom of L^- and two acetate groups. In **1′**–**5′** the Cu^{II} is bound to the bidentate arm and has a square-pyramidal geometry with one acetate oxygen at the apical site. The M^{II} is bound to the tridentate arm and has a six-coordinate geometry together with two acetate oxygen atoms. In the case of **7′** the Zn is bound to the bidentate arm and the Ni is bound to the tridentate arm. **8**·2-PrOH (**8′**) has a dinuclear core bridged by the phenolic oxygen atom of L^- and one acetate group. The Cu bound to the bidentate arm has a square-pyramidal geometry with an isothiocyanate group at the apical site. The Ni bound to the tridentate arm has a six-coordinate geometry with further coordination of an isothiocyanate group. The site specificity of the metal ions is discussed together with the crystal structure of $[Cu_4(L)_2(AcO)_3](ClO_4)_3 \cdot H_2O$ (**9**) prepared in this work.

Introduction

Bimetallic cores have been recognized at the active sites of many metalloenzymes[1] and model studies with simple dinuclear metal complexes are becoming increasingly important in understanding biological functions of the bimetallic cores. Phenol-based "end-off" compartmental ligands, possessing chelating arms attached to the 2 and 6 positions of the phenolic ring (Chart 1), have often been used for modeling bimetallic biosites.[2−6] μ-Phenoxodi(μ-carboxylato)-dimanganese(II)[2] and μ-phenoxodi(μ-carboxylato)dizinc(II)[3] complexes of type A ligands were investigated as functional models of Mn catalase and phosphatase, respectively. Urea adducts of dinuclear nickel complexes derived from type A and B ligands were studied as relevance to urease−urea interaction,[5,6] and conversion of urea into cyanate ion (NCO^-) was achieved on dinuclear nickel(II) complexes.[6] Type C ligands having two tridentate chelating arms have been used for model studies of non-heme bimetallic biosites.[4]

Chart 1. Three Types of "End-Off" Compartmental Ligands

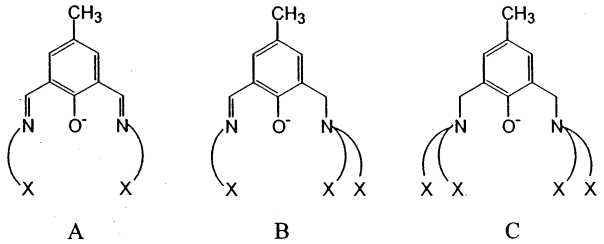

* Authors to whom correspondence should be addressed. E-mail: okawascc@mbox.nc.kyushu-u.ac.jp.

(1) (a) Fenton, D. E.; Ōkawa, H. *Perspectives on Bioinorganic Chemistry*; JAI Press: London, UK, 1993; Vol. 2, p 81. (b) Karlin, K. D. *Science* **1993**, *261*, 701.

(2) (a) Sakiyama, H.; Ōkawa, H.; Isobe, R. *J. Chem. Soc., Chem. Commun.* **1993**, 882. (b) Sakiyama, H.; Tamaki, H.; Kodera, M.; Matsumoto, N.; Ōkawa, H. *J. Chem. Soc., Dalton Trans.* **1993**, 591. (c) Sakiyama, H.; Ōkawa, H.; Suzuki, M. *J. Chem. Soc., Dalton Trans.* **1993**, 3832. (d) Higuchi, C.; Sakiyama, H.; Ōkawa, H.; Isobe, R.; Fenton, D. E. *J. Chem. Soc., Dalton Trans.* **1994**, 1097. (e) Higuchi, C.; Sakiyama, H.; Ōkawa, H.; Fenton, D. E. *J. Chem. Soc., Dalton Trans.* **1995**, 4015.

(3) Abe, K.; Izumi, J.; Ohba, M.; Yokoyama, T.; Ōkawa, H. *Bull. Chem. Soc. Jpn.* **2001**, *74*, 85.

(4) Suzuki, M.; Furutachi, H.; Ōkawa, H. *Coord. Chem. Rev.* **2000**, *200*−*202*, 105.

(5) Koga, T.; Furutachi, H.; Nakamura, H.; Fukita, N.; Ohba, M.; Takahashi, K.; Ōkawa, H. *Inorg. Chem.* **1998**, *37*, 989.

(6) Uozumi, S.; Furutachi, H.; Ohba, M.; Ōkawa, H.; Fenton, D. E.; Shindo, K.; Murata, S.; Kitko, D. J. *Inorg. Chem.* **1998**, *37*, 6281.

10.1021/ic020002f CCC: $22.00
Published on Web 07/30/2002

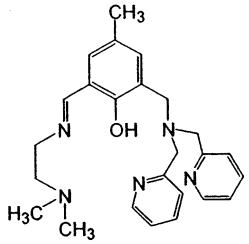

Figure 1. Chemical structure of HL.

Recently, heterodinuclear cores were recognized at the active sites of some metalloenzymes such as purple acid phosphatase (FeZn),[7] human calcineurin (FeZn),[8] and human protein phosphatase 1 (FeMn).[9] It is considered that these biological systems employ a heterodinuclear core to realize a specific function by the conjunction of distinct roles of two kinds of metal ions. We are interested in functional models of heterobimetallic phosphatases.[10] Type C compartmental ligands are known to afford some heterodinuclear complexes,[11−14] but type B ligands must be more suitable for our purpose because of its unsymmetrical nature. In this work a type B compartmental ligand, 2-{*N*-[2-(dimethylamino)-ethyl]iminomethyl}-6-[*N*,*N*-di(2-pyridylmethyl)aminomethyl]-4-methylphenol (HL, Figure 1), is used to afford the following heterodinuclear complexes: $[CuMn(L)(AcO)_2]ClO_4$ (**1**), $[CuFe(L)(AcO)_2]ClO_4$ (**2**), $[CuCo(L)(AcO)_2]ClO_4$ (**3**), $[CuNi(L)(AcO)_2]ClO_4$ (**4**), $[CuZn(L)(AcO)_2]ClO_4$ (**5**), $[ZnCo(L)(AcO)_2]ClO_4$ (**6**), $[ZnNi(L)(AcO)_2]ClO_4$ (**7**), and $[CuNi(L)(AcO)(NCS)_2]$ (**8**). Site specificity of metal ions is discussed based on X-ray crystallographic, mass spectrometric, and electronic spectral studies for the complexes. In this paper, the site specificities of metal ions are designated as $[M_aM_b(L)(AcO)_2]ClO_4$ or "M_aM_b complex", where the first metal (M_a) is bound to the bidentate arm and the second metal (M_b) is bound to the tridentate arm.

Experimental Section

Physical Measurements. Elemental analyses of C, H, and N were obtained at the Elemental Analysis Service Center of Kyushu University. Metal analyses were made on a Shimadzu AA-660 atomic absorption/flame emission spectrometer. Infrared spectra were recorded on a Perkin-Elmer BX FT-IR system with KBr disk. Electronic absorption spectra were recorded in *N*,*N*-dimethylformamide (DMF) on a Shimadzu UV-3100PC spectrometer. Molar conductances were measured at $\sim 1 \times 10^{-3}$ M concentration in DMF with a DKK AOL-10 conductivity meter at 20 °C. Fast atom bombardment (FAB) mass spectra were recorded on a JEOL JMS-SX/SX 102A tandem mass spectrometer with *m*-nitrobenzyl alcohol as the matrix. Magnetic susceptibilities were measured on a Quantum Design MPMS2 SQUID susceptometer.

Preparation. 3-[*N*,*N*-Di(2-pyridylmethyl)aminomethyl]-5-methylsalicylaldehyde (HL′) was prepared by the method in our previous paper.[15] Other chemicals were of reagent grade and were used as purchased.

$[CuMn(L)(AcO)_2]ClO_4$ (1). The ligand HL was prepared in situ by reacting HL′ (0.174 g, 0.5 mmol) and *N*,*N*-dimethylethylenediamine (44 mg, 0.5 mmol) in methanol (5 cm^3) at the reflux temperature. To the ligand solution were added copper(II) acetate monohydrate (100 mg, 0.5 mmol) and manganese(II) acetate tetrahydrate (139 mg, 0.5 mmol), and the mixture was refluxed for 30 min. Then, sodium perchlorate (122 mg, 1.0 mmol) was added and the solution was diffused with ether to afford green crystals. Yield: 250 g (66.5%). Anal. Calcd for $C_{29}ClCuH_{36}MnN_5O_9$: C, 46.28; H; 4.82, N, 9.31; Cu, 8.44; Mn, 7.30. Found: C, 46.46; H, 5.02; N, 9.07; Cu, 8.22; Mn, 6.90. μ_{eff} per CuMn: 5.82 μ_B at 298 K. Selected IR data (ν/cm^{-1}) with KBr disk: 1638, 1595, 1427, 1306, 1090, 1015, 776, 623. Molar conductance (Λ_M/S cm^2 mol^{-1}) in DMF: 64.

$[CuFe(L)(AcO)_2]ClO_4$ (2). 2 was prepared as green crystals in a manner similar to that for **1**, using iron(II) acetate heptahydrate instead of manganese(II) acetate tetrahydrate. Yield: 245 mg (65.0%). Anal. Calcd for $C_{29}ClCuFeH_{36}N_5O_9$: C, 46.23; H; 4.82, N, 9.29; Cu, 8.43; Fe, 7.44. Found: C, 45.98; H, 4.82; N, 9.35; Cu, 9.5; Fe, 6.0. μ_{eff} per CuFe: 5.02 μ_B at 298 K. Selected IR data (ν/cm^{-1}) with KBr disk: 1636, 1602, 1428, 1304, 1198, 1113, 776, 621. Molar conductance (Λ_M/S cm^2 mol^{-1}) in DMF: 63.

$[CuCo(L)(AcO)_2]ClO_4$ (3). 3 was prepared as green crystals in a manner similar to that for **1**, using cobalt(II) acetate tetrahydrate instead of manganese(II) acetate tetrahydrate. Yield: 230 mg (55.5%). Anal. Calcd for $C_{29}ClCoCuH_{36}N_5O_9$: C, 46.04; H, 4.80; N, 9.26; Cu, 8.40; Co, 7.79. Found: C, 45.93; H, 4.91; N, 9.13; Cu, 8.00; Co, 7.35. μ_{eff} per CuCo: 5.12 μ_B at 298 K. Selected IR data (ν/cm^{-1}) with KBr disk: 1638, 1605, 1418, 1302, 1089, 1019, 775, 624. Molar conductance (Λ_M/S cm^2 mol^{-1}) in DMF: 60.

$[CuNi(L)(AcO)_2]ClO_4$ (4). 4 was obtained as green crystals in a manner similar to that for **1**, using nickel(II) acetate tetrahydrate instead of manganese(II) acetate tetrahydrate. Yield: 220 g (58.2%). Anal. Calcd for $C_{29}ClCuH_{36}N_5NiO_9$: C, 46.05; H, 4.80; N, 9.01; Cu, 8.40; Ni, 7.76. Found: C, 46.09; H, 4.87; N, 9.01; Cu, 8.00; Ni, 7.13. μ_{eff} per CuNi: 3.55 μ_B at 298 K. Selected IR data (ν/cm^{-1}) with KBr disk: 1637, 1602, 1416, 1304, 1093, 1017, 775, 623. Molar conductance (Λ_M/S cm^2 mol^{-1}) in DMF: 60.

$[CuZn(L)(AcO)_2]ClO_4$ (5). 5 was obtained as green crystals in a manner similar to that for **1**, using zinc(II) acetate dihydrate instead of manganese(II) acetate tetrahydrate. Yield: 210 mg (55.0%). Anal. Calcd for $C_{29}ClCuH_{36}N_5O_9Zn$: C, 45.69; H, 4.76; N, 9.18; Cu, 8.33; Zn, 8.57. Found: C, 45.69; H, 4.76; N, 9.20; Cu, 9.40; Zn, 6.90. μ_{eff} per Cu: 1.85 μ_B at 298 K. Selected IR data (ν/cm^{-1}) with KBr disk: 1637, 1604, 1428, 1308, 1094, 1018, 774, 623. Molar conductance (Λ_M/S cm^2 mol^{-1}) in DMF: 60.

$[ZnCo(L)(AcO)_2]ClO_4$ (6). A solution of HL was prepared by reacting HL′ (174 mg, 0.5 mmol) and *N*,*N*-dimethylethylenediamine (44 mg, 0.5 mmol) in hot methanol (5 cm^3). To the resulting yellow solution were added zinc(II) acetate dihydrate (110 mg, 0.5 mmol)

(7) Sträter, N.; Klabunde, T.; Tucker, P.; Witzel, H.; Krebs, B. *Science* **1995**, *268*, 1489.
(8) Kissinger, C. R.; Parge, H. E.; Knighton, D. R.; Llewis, C. T.; Pelletier, L. A.; Tempczyk, A.; Kalish, V. J.; Tucker, K. D.; Showalter, R. E.; Moomaw, E. W.; Gastinel, L. N.; Habuka, N.; Chen, X. Y.; Maldonado, F.; Barker, J. E.; Bayquet, R.; Villafranca, J. E. *Nature* **1995**, *378*, 641.
(9) Egloff, M.-P.; Cohen, P. T. W.; Reinemer, P.; Barford, D. *J. Mol. Biol.* **1995**, *254*, 942.
(10) Arimura, K.; Ohba, M.; Yokoyama, T.; Ōkawa, H. *Chem. Lett*. **2001**, 1134.
(11) Borovik, A. S.; Papaefthymiou, V.; Taylor, L. F.; Anderson, O. P.; Que, L., Jr. *J. Am. Chem. Soc*. **1989**, *111*, 6183.
(12) Holman, T. R.; Juarez-Garcia, C.; Hendrich, M. P.; Que, L., Jr.; Münck, E. *J. Am. Chem. Soc*. **1990**, *112*, 7611.
(13) Juarez-Garcia, C.; Hendrich, M. P.; Holman, T. R.; Que, L., Jr.; Münck, E. *J. Am. Chem. Soc*. **1991**, *113*, 518.
(14) Suzuki, M.; Fujinami, S.; Hibino, T.; Hori, H.; Maeda, Y.; Uehara, A.; Suzuki, M. *Inorg. Chim. Acta* **1998**, *283*, 124.
(15) Uozumi, S.; Ohba, M.; Ōkawa, H.; Fenton, D. E. *Chem. Lett*. **1997**, 673.

and cobalt(II) acetate tetrahydrate (124 mg, 0.5 mmol), and the mixture was further refluxed for 30 min. After the addition of sodium perchlorate (122 mg, 1.0 mmol), the mixture was diffused with ether to form brown crystals. Yield: 225 mg (63.6%). Anal. Calcd for $C_{31}ClCoH_{44}N_5O_{11}Zn$: C, 45.27; H, 5.39; N, 8.51; Zn, 7.95; Co, 7.17. Found: C, 45.49; H, 5.10; N, 8.39; Zn, 7.88 Co, 7.51. μ_{eff} per ZnCo: 4.63 μ_B at 298 K. Selected IR data (ν/cm^{-1}) with KBr disk: 1637, 1605, 1430, 1310, 1090, 1019, 776, 624. Molar conductance (Λ_M/S cm^2 mol^{-1}) in DMF: 65.

[ZnNi(L)(AcO)$_2$]ClO$_4$ (7). **7** was obtained as light green crystals in a manner similar to that for **6**. Yield: 230 mg (60.9%). Anal. Calcd for $C_{29}ClH_{36}N_5NiO_9Zn$: C, 45.94; H, 4.79; N, 9.24; Zn, 8.62; Ni, 7.74. Found: C, 45.79; H, 4.79; N, 9.27; Zn, 9.17; Ni, 6.87. μ_{eff} per ZnNi: 3.10 μ_B at 298 K. Selected IR data (n/cm^{-1}) with KBr disk: 1637, 1603, 1431, 1312, 1093, 1022, 775, 624. Molar conductance (Λ_M/S cm^2 mol^{-1}) in DMF: 73.

[CuNi(L)(AcO)(NCS)$_2$] (8). **8** was obtained as green crystals in a manner similar to that of **4** except for the use of sodium thiocyanate in stead of sodium acetate. Yield: 260 mg (72.8%). Anal. Calcd for $C_{29}CuH_{33}N_7NiO_3S_2$: C, 48.79; H, 4.66; N, 13.73; Cu, 8.22; Ni, 8.89. Found: C, 48.59; H, 4.69; N, 13.63; Cu, 8.16; Ni, 8.90. μ_{eff} per CuNi: 3.55 μ_B at 298 K. Selected IR data (ν/cm^{-1}) with KBr disk: 2067, 1639, 1606, 1569, 1421, 1303, 1020, 766. Molar conductance (Λ_M/S cm^2 mol^{-1}) in DMF: 74.

[Cu$_4$(L)$_2$(AcO)$_3$](ClO$_4$)$_3$·H$_2$O (9). **9** was prepared by the reaction of HL and 2 equiv of Cu(II) acetate monohydrate in the presence of sodium perchlorate. Yield: 250 mg (66.5%). Anal. Calcd for $C_{56}Cl_3Cu_4H_{72}N_{10}O_{20}$: C, 42.96; H; 4.63, N, 8.95; Cu, 16.23. Found: C, 42.79; H, 4.46; N, 8.99; Cu, 16.06.

X-ray Structure Analyses. Single crystals of **1**·MeOH (**1′**), **2**·MeOH (**2′**), **3**·MeOH (**3′**), **4**·MeOH (**4′**), **5**·MeOH (**5′**), and **7**·MeOH (**7′**) were grown from a methanol solution of each complex. Single crystals of **8**·2-PrOH (**8′**) were grown when a DMF solution of **8** was diffused with 2-propanol (2-PrOH). Each single crystal of **1′**−**5′**, **7′**, **8′**, and [Cu$_4$(L)$_2$(AcO)$_3$](ClO$_4$)$_3$·H$_2$O (**9**) was sealed in a capillary tube and used for X-ray crystallographic measurements on a Rigaku AFC-7R diffractometer, using graphite monochromated Mo Kα radiation (λ = 0.71069 Å) and a 12 kW rotating anode generator. The data were collected at 23 ± 1 °C with use of an $\omega-2\theta$ scan technique at a scan rate of 16.0°/min (in ω).

Three standard reflections were monitored every 150 reflections, and a linear correction factor was applied to the data to account for decay phenomena observed. Intensity data were corrected for Lorentz and polarization effects. The structures were solved by the direct method and expanded with Fourier techniques. The non-hydrogen atoms were refined anisotropically. Hydrogen atoms were included in the structure factor calculation but not refined. Computations were carried out on an IRIS O2 computer with use of the TEXAN crystallographic software package.[16]

Results and Discussions

FAB Mass Spectrometric Characterization. Dinuclear complexes of the general formula [M$_a$M$_b$(L)(AcO)$_2$]ClO$_4$ (M$_a$M$_b$ = Cu^{II}Mn^{II} (**1**), Cu^{II}Fe^{II} (**2**), Cu^{II}Co^{II} (**3**), Cu^{II}Ni^{II} (**4**), Cu^{II}Zn^{II} (**5**), Zn^{II}Co^{II} (**6**), and Zn^{II}Ni^{II} (**7**)), were obtained by one-pot reaction of HL, M$_a$(II) acetate, and M$_b$(II) acetate (1:1:1) in methanol in the presence of sodium perchlorate. The assignment of "CuM" for **1**−**5** and **8** and the assignment of "ZnM" for **6** and **7** are based on X-ray crystallographic studies as discussed later. The FAB mass spectrometric result for **1** is given in Figure 2 (trace a). It shows parent ion peaks centered around *m*/*z* 652 that can be attributed to {CuMn(L)(AcO)$_2$}$^+$ by taking into consideration the natural abundance of isotopic ^{63}Cu (69.09%) and ^{65}Cu (30.91%). No ion peak due to homodinuclear species was detected. Similarly, the FAB mass spectrometric studies for **2**−**5** demonstrate that they have a discrete heterodinuclear core. The FAB mass for **6** (Figure 1, trace b), on the other hand, showed weak signals attributable to homodinuclear {CoCo(L)(AcO)$_2$}$^+$ (*m*/*z* 652) and {ZnZn(L)(AcO)$_2$}$^+$ (*m*/*z* 666), in addition to the main signals due to [ZnCo(L)(AcO)$_2$]$^+$ centered around *m*/*z* 659. The result indicates a partial disproportionation of **6** in solution. Similarly, the FAB mass studies for **7** (ZnNi) indicated a partial disproportionation into the homodinuclear Ni$_2$ and Zn$_2$ species. [CuNi(L)(AcO)(NCS)$_2$] (**8**) showed ion peaks centered around *m*/*z* 656 attributable to {CuNi(L)(AcO)(NCS)}$^+$; no ion peak due to the homodinuclear species was detected.

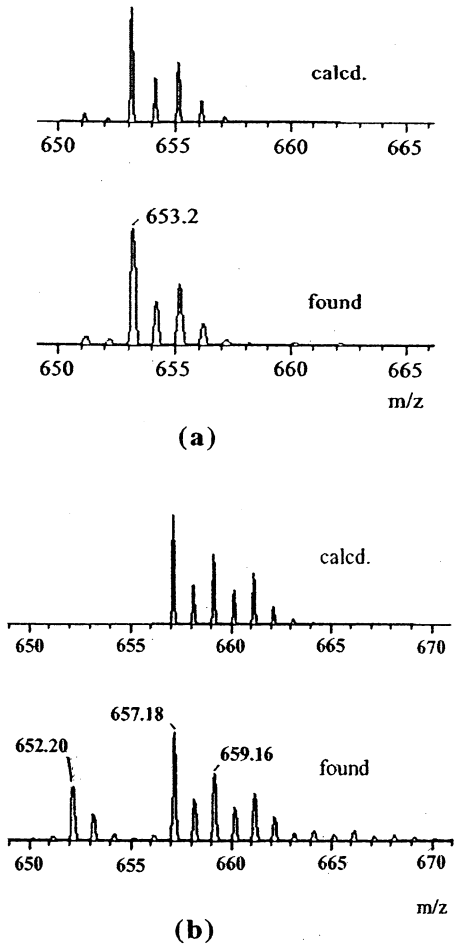

Figure 2. FAB mass spectra of (a) [CuMn(L)(AcO)$_2$]ClO$_4$ (**1**) and (b) [ZnCo(L)(AcO)$_2$]ClO$_4$ (**6**).

Crystal Structures: (a) [CuM(L)(AcO)$_2$]ClO$_4$·MeOH (1′−5′) and [ZnNi(L)(AcO)$_2$]ClO$_4$·MeOH (7′). **1′**−**5′** and **7′** are isostructural. An ORTEP[17] view of **1′** is given in Figure

(16) TEXAN, Molecular Structure Analysis Package, Molecular Structure Corporation, Houston, TX, 1985 and 1992.

(17) Johnson, C. K. Report 3794, Oak Ridge National Laboratory, Oak Ridge, TN, 1965.

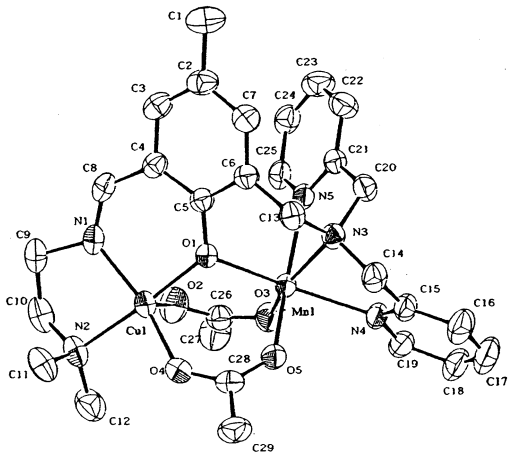

Figure 3. An ORTEP view of $[CuMn(L)(AcO)_2]ClO_4$ (**1**) with the atom numbering scheme.

Table 1. Selected Bond Lengths (Å) and Angles (deg) for $[CuMn(L)(AcO)_2]ClO_4 \cdot MeOH$ (**1′**)

	Distances		
Cu−O(1)	1.929(3)	Mn−O(1)	2.209(3)
Cu−O(2)	2.281(4)	Mn−O(3)	2.091(4)
Cu−O(4)	1.943(4)	Mn−O(5)	2.136(4)
Cu−N(1)	1.946(4)	Mn−N(3)	2.313(4)
Cu−N(2)	2.040(4)	Mn−N(4)	2.250(4)
Cu···Mn	3.296(1)	Mn−N(5)	2.298(4)
	Angles		
Cu−O(1)−Mn	105.4(1)	O(1)−Mn−N(3)	85.1(1)
O(1)−Cu−O(2)	96.5(1)	O(1)−Mn−N(4)	153.2(1)
O(1)−Cu−O(4)	92.5(1)	O(1)−Mn−N(5)	92.2(1)
O(1)−Cu−N(1)	92.2(2)	O(3)−Mn−O(5)	104.1(2)
O(1)−Cu−N(2)	173.2(2)	O(3)−Mn−N(3)	157.8(1)
O(2)−Cu−O(4)	107.7(2)	O(3)−Mn−N(4)	93.4(2)
O(2)−Cu−N(1)	92.5(2)	O(3)−Mn−N(5)	90.8(1)
O(2)−Cu−N(2)	89.5(2)	O(5)−Mn−N(3)	91.9(1)
O(4)−Cu−N(1)	158.6(2)	O(5)−Mn−N(4)	83.3(1)
O(4)−Cu−N(2)	88.8(2)	O(5)−Mn−N(5)	165.1(1)
N(1)−Cu−N(2)	84.2(2)	N(3)−Mn−N(4)	73.0(1)
O(1)−Mn−O(3)	111.9(1)	N(3)−Mn−N(5)	73.8(1)
O(1)−Mn−O(5)	82.1(1)	N(4)−Mn−N(5)	96.3(1)

Table 2. Selected Bond Lengths (Å) for $[CuM(L)(AcO)_2]ClO_4 \cdot MeOH$ (M = Fe (**2′**), Co (**3′**), Ni (**4′**), Zn (**5′**))

	M =			
distances	Fe (**2′**)	Co (**3′**)	Ni (**4′**)	Zn (**5′**)
Cu−O(1)	1.923(2)	1.934(3)	1.928(2)	1.940(3)
Cu−O(2)	2.264(3)	2.232(4)	2.195(3)	2.220(3)
Cu−O(4)	1.940(3)	1.941(4)	1.946(3)	1.943(3)
Cu−N(1)	1.955(3)	1.960(4)	1.959(3)	1.961(4)
Cu−N(2)	2.047(3)	2.058(4)	2.056(3)	2.048(4)
M−O(1)	2.166(2)	2.114(3)	2.098(3)	2.145(3)
M−O(3)	2.011(3)	2.018(4)	2.014(3)	2.004(3)
M−O(5)	2.114(3)	2.098(4)	2.056(3)	2.083(3)
M−N(3)	2.227(3)	2.167(4)	2.112(3)	2.217(4)
M−N(4)	2.187(3)	2.143(4)	2.093(3)	2.161(3)
M−N(5)	2.207(3)	2.160(4)	2.098(3)	2.206(3)
Cu···M	3.298(1)	3.302(1)	3.318(1)	3.311(1)

3 together with the atom numbering scheme. The relevant bond distances and angles for **1′** are given in Table 1 and the selected bond distances for **2′**−**5′** are summarized in Table 2. The relevant bond distances and angles for **7′** are given in Table 3.

The Cu is bound to the bidentate arm and the Mn is bound to the tridentate arm. The metal ions are bridged by the phenolic oxygen of L^- and two acetate groups. The Cu··· Mn intermetallic separation is 3.301(1) Å. The geometry around the Cu is best depicted as square pyramid with O(1), N(1), and N(2) of L^- and one acetate oxygen O(4) on the equatorial base and with another acetate oxygen O(2) at the apical site. The Cu-to-donor bond distances on the equatorial base range from 1.914(5) to 2.033(7) Å. The axial Cu−O(2) bond (2.288(6) Å) is elongated owing to the Jahn−Teller effect for d^9 electronic configuration.[18] The Cu is 0.224 Å displaced from the basal least-squares plane toward the axial O(2). The geometry about the Mn is nearly octahedral. One pyridine nitrogen N(4) is located cis to the bridging phenolic oxygen O(1) and another pyridine nitrogen N(5) is trans to the phenolic oxygen. The basal $\{CuN_2O_2\}$ entity and the aromatic ring are not coplanar: the dihedral angle between the two least-squares planes is 17.7°. The sum of the Cu−O(1)−Mn, Cu−O(1)−C(5), and Mn−O(1)−C(5) angles is 351.4°, indicating a nonplanar configuration about the bridging phenolic oxygen.

Table 3. Selected Bond Lengths (Å) and Angles (deg) for $[ZnNi(L)(AcO)_2]ClO_4 \cdot MeOH$ (**7′**)

	Distances		
Zn−O(1)	2.020(3)	Ni−O(1)	2.073(3)
Zn−O(2)	1.997(4)	Ni−O(3)	2.053(3)
Zn−O(4)	1.980(4)	Ni−O(5)	2.059(3)
Zn−N(1)	2.072(4)	Ni−N(3)	2.125(4)
Zn−N(2)	2.162(4)	Ni−N(4)	2.106(4)
Zn···Ni	3.268(1)	Ni−N(5)	2.116(4)
	Angles		
Zn−O(1)−Ni	106.0(1)	O(1)−Ni−N(3)	91.8(1)
O(1)−Zn−O(2)	105.6(1)	O(1)−Ni−N(4)	165.9(1)
O(1)−Zn−O(4)	91.8(1)	O(1)−Ni−N(5)	90.6(1)
O(1)−Zn−N(1)	87.5(1)	O(3)−Ni−O(5)	96.9(1)
O(1)−Zn−N(2)	159.6(2)	O(3)−Ni−N(3)	164.8(1)
O(2)−Zn−O(4)	110.8(2)	O(3)−Ni−N(4)	90.3(1)
O(2)−Zn−N(1)	103.9(2)	O(3)−Ni−N(5)	91.1(1)
O(2)−Zn−N(2)	93.0(2)	O(5)−Ni−N(3)	92.5(1)
O(4)−Zn−N(1)	144.1(2)	O(5)−Ni−N(4)	84.3(1)
O(4)−Zn−N(2)	89.4(2)	O(5)−Ni−N(5)	171.8(1)
N(1)−Zn−N(2)	79.8(2)	N(3)−Ni−N(4)	78.7(1)
O(1)−Ni−O(3)	100.8(1)	N(3)−Ni−N(5)	80.3(1)
O(1)−Ni−O(5)	85.8(1)	N(4)−Ni−N(5)	97.9(1)

In the series of $Cu^{II}M^{II}$ complexes (**1′**−**5′**), the average of the M-to-donor distances decreases in the following order: **1′** (M = Mn, 2.217 Å) > **2′** (Fe, 2.150 Å) > **5′** (Zn, 2.135 Å) > **3′** (Co, 2.113 Å) > **4′** (Ni, 2.077 Å). This order is in accord with the decreasing order in ionic radius of octahedral M^{II}: Mn^{II} (0.96 Å) > Fe^{II} (0.91 Å) > Zn^{II} (0.89 Å) > Co^{II} (0.88 Å) > Ni^{II} (0.84 Å).[19] The displacement of the Cu from the basal N_2O_2 least-squares plane increases in the same order of M: **1′** (0.224 Å) < **2′** (0.239 Å) < **5′** (0.242 Å) ∼ **3′** (0.242 Å) < **4′** (0.255 Å). The sum of the Cu−O(1)−M, Cu−O(1)−C(5), and M−O(1)−C(5) angles about the bridging phenolic oxygen atom also increases in the same order: **1′** (351.4°) < **2′** (353.0°) < **5′** (354.6°) < **3′** (354.7°) < **4′** (357.3°). On the other hand, the Cu···M separation is not in harmony with the order of the ionic radius of M^{II} and increases in the following order: **4′** (3.268(1) Å) < **1′** (3.295(1) Å) < **2′** (3.298(1) Å) < **3′** (3.302(1) Å) < **5′** (3.311(1) Å).

(18) Jahn, H. A.; Teller, E. *Proc. R. Soc. London* **1937**, *A161*, 220.
(19) Shannon, R. D.; Prewitt, C. T. *Acta Crystallogr.* **1969**, *B25*, 925.

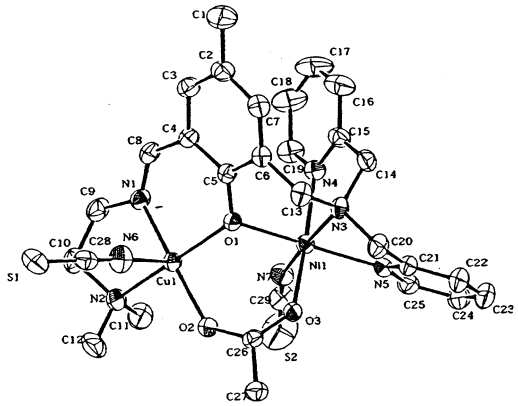

Figure 4. An ORTEP view of [CuNi(L)(AcO)(NCS)$_2$]MeOH (**8′**) with the atom numbering scheme.

In complex **7′** the metal bound to the bidentate arm has an average bond distance of 2.049 Å and the metal bound to the tridentate arm has an average bond distance of 2.088 Å. The latter bond distance is compared to the average bond distance of the Ni in **4′** (2.078 Å) but differs largely from the average bond distance of the Zn in **5′** (2.135 Å). This fact suggests the "ZnNi" core for **7′**. The site specificity of metal ions is supported by the structures of analogous [Zn_2(L)(AcO)$_2$]ClO_4[3] and [Ni_2(L)(AcO)$_2$(MeOH)]PF_6.[6] That is, the Zn bound to the bidentate arm in the former has an average bond distance of 2.049 Å and the Ni bound to the tridentate arm in the latter has an average bond distance of 2.073 Å. These bond distances are compatible with the structure of **7′**. It must be mentioned that the Ni bound to the bidentate arm of [Ni_2(L)(AcO)$_2$(MeOH)]PF_6 has an average bond distance of 2.082 Å and the Zn bound to the tridentate arm of [Zn_2(L)(AcO)$_2$]ClO_4 has an average bond distance of 2.129 Å. Evidently the "NiZn" core is not the case for **7′**. It is supposed that **6** has the "ZnCo" core from the analogy to **7′**.

(b) [CuNi(L)(AcO)(NCS)$_2$]·2-PrOH (8′). An ORTEP view of **8′** is given in Figure 4 together with the numbering scheme. The selected bond distances and angles are summarized in Table 4.

The Cu is bound to the bidentate arm and the Ni is bound to the tridentate arm in the Cu···Ni separation of 3.402(1) Å. The Cu assumes a square-pyramidal geometry with O(1), N(1), and N(2) of L^- and O(2) of the bridging acetate group on the base and N(6) of thiocyanate ion at the apex. The in-plane Cu-to-donor bond distances range from 1.928(2) to 2.063(3) Å. The axial Cu−N(6) bond distance is elongated (2.272(4) Å). The Cu is 0.212 Å displaced from the basal least-squares plane toward N(6). The Ni has a six-coordinate geometry with further coordination of an isothiocyanate nitrogen N(7). The Ni-to-donor bond distances range from 2.035(3) to 2.112(3) Å. The sum of the Cu−O(1)−Ni, Cu−O(1)−C(5), and Ni−O(1)−C(5) angles is 356.6°, which is slightly larger than those for **1′**−**5′**.

Site Specificity of Metal Ions. The crystal structure of a dinuclear Cu complex of L^- must be informative for inspecting the site specificity of metal ions in **1**−**5**. Contrary to our expectation, [Cu_4(L)$_2$(AcO)$_3$](ClO_4)$_3$·H_2O (**9**) was obtained in this work. Eventually, it has proved of value to understand the site specificity of metal ions in **1**−**5**. An ORTEP view of **9** is shown in Figure 5 and the selected bond distances and angles are summarized in Table 5. It has a "dimer-of-dimers" structure comprised of two dissimilar {Cu_2(L)(AcO)}$^{2+}$ units (A and B) combined by another acetate group (Figure 5a). In the unit A, two Cu atoms (Cu(1) and Cu(2)) are doubly bridged by the phenolic oxygen atom O(1) and an acetate group (Figure 5b). The geometry around Cu(1) is best depicted as a square pyramid and the geometry about Cu(2) is also depicted as a square pyramid. In unit B, two Cu atoms (Cu(3) and Cu(4)) are singly bridged by the phenolic oxygen atom O(6) (Figure 5c). The Cu(3) bound to the bidentate arm assumes a planar geometry together with the acetate oxygen O(5). The geometry around Cu(4) is square pyramidal together with a unidentate acetate group. The two {Cu_2(L)(AcO)}$^{2+}$ units are linked by the Cu(1)−O(4)−C(28)(C(29))−O(5)−Cu(3) linkage. The average of the in-plane Cu-to-donor distances for Cu(1) and Cu(3), bound to the bidentate arm of L^-, is 1.990 and 1.956 Å, respectively. The above X-ray crystallographic result indicates that the "$M^{II}Cu^{II}$" core is hardly formed because the Cu bound to the tridentate arm prefers a five-coordinate geometry.

The site specificity of metal ions in [M_aM_b(L)(AcO)$_2$]$^+$ is associated with the ligand L^- that affords a five-coordinate geometry for the M_a bound to the bidentate arm and a six-

Table 4. Selected Bond Lengths (Å) and Angles (deg) for [CuNi(L)(AcO)(NCS)$_2$](2-PrOH)$_{0.5}$ (**8′**)

		Distances	
Cu−O(1)	1.930(3)	Ni−O(1)	2.081(2)
Cu−O(2)	1.949(3)	Ni−O(3)	2.052(3)
Cu−N(1)	1.970(3)	Ni−N(3)	2.112(3)
Cu−N(2)	2.067(3)	Ni−N(4)	2.112(3)
Cu−N(6)	2.272(4)	Ni−N(5)	2.092(3)
Cu···Ni	3.401(1)	Ni−N(7)	2.033(4)
		Angles	
Cu−O(1)−Ni	115.9(1)	O(1)−Ni−N(4)	164.3(1)
O(1)−Cu−O(2)	93.2(1)	O(1)−Ni−N(5)	89.4(1)
O(1)−Cu−N(1)	89.6(1)	O(1)−Ni−N(7)	98.4(1)
O(1)−Cu−N(2)	165.5(1)	O(3)−Ni−N(3)	93.8(1)
O(1)−Cu−N(6)	100.2(1)	O(3)−Ni−N(4)	86.5(1)
O(2)−Cu−N(1)	168.2(1)	O(3)−Ni−N(5)	173.0(1)
O(2)−Cu−N(2)	90.4(1)	O(3)−Ni−N(7)	92.0(1)
O(2)−Cu−N(6)	96.8(1)	N(3)−Ni−N(4)	77.4(1)
N(1)−Cu−N(2)	84.2(1)	N(3)−Ni−N(5)	80.8(1)
N(1)−Cu−N(6)	93.9(1)	N(3)−Ni−N(7)	170.7(1)
N(2)−Cu−N(6)	93.3(1)	N(4)−Ni−N(5)	96.6(1)
O(1)−Ni−O(3)	86.0(1)	N(4)−Ni−N(7)	95.7(1)
O(1)−Ni−N(3)	89.3(1)	N(5)−Ni−N(7)	93.9(1)

Table 5. Selected Bond Lengths (Å) for [Cu_4(L)$_2$(AcO)$_3$](ClO_4)$_3$·H_2O (**9**)

Cu(1)−O(1)	1.938(4)	Cu(3)−O(5)	1.946(4)
Cu(1)−O(2)	2.022(4)	Cu(3)−O(6)	1.919(4)
Cu(1)−O(4)	2.242(4)	Cu(3)−N(6)	1.920(5)
Cu(1)−N(1)	1.948(6)	Cu(3)−N(7)	2.038(5)
Cu(1)−N(2)	2.051(5)	Cu(4)−O(6)	2.259(4)
Cu(2)−O(1)	2.270(4)	Cu(4)−O(7)	1.946(4)
Cu(2)−O(3)	1.931(4)	Cu(4)−N(8)	2.048(5)
Cu(2)−N(3)	2.021(5)	Cu(4)−N(9)	1.992(6)
Cu(2)−N(4)	2.015(5)	Cu(4)−N(10)	1.982(5)
Cu(2)−N(5)	1.992(4)		
Cu(1)···Cu(2)	3.592(1)	Cu(2)···Cu(3)	7.052(1)
Cu(1)···Cu(3)	4.622(1)	Cu(2)···Cu(4)	9.674(1)
Cu(1)···Cu(4)	7.131(1)	Cu(3)···Cu(4)	3.512(1)

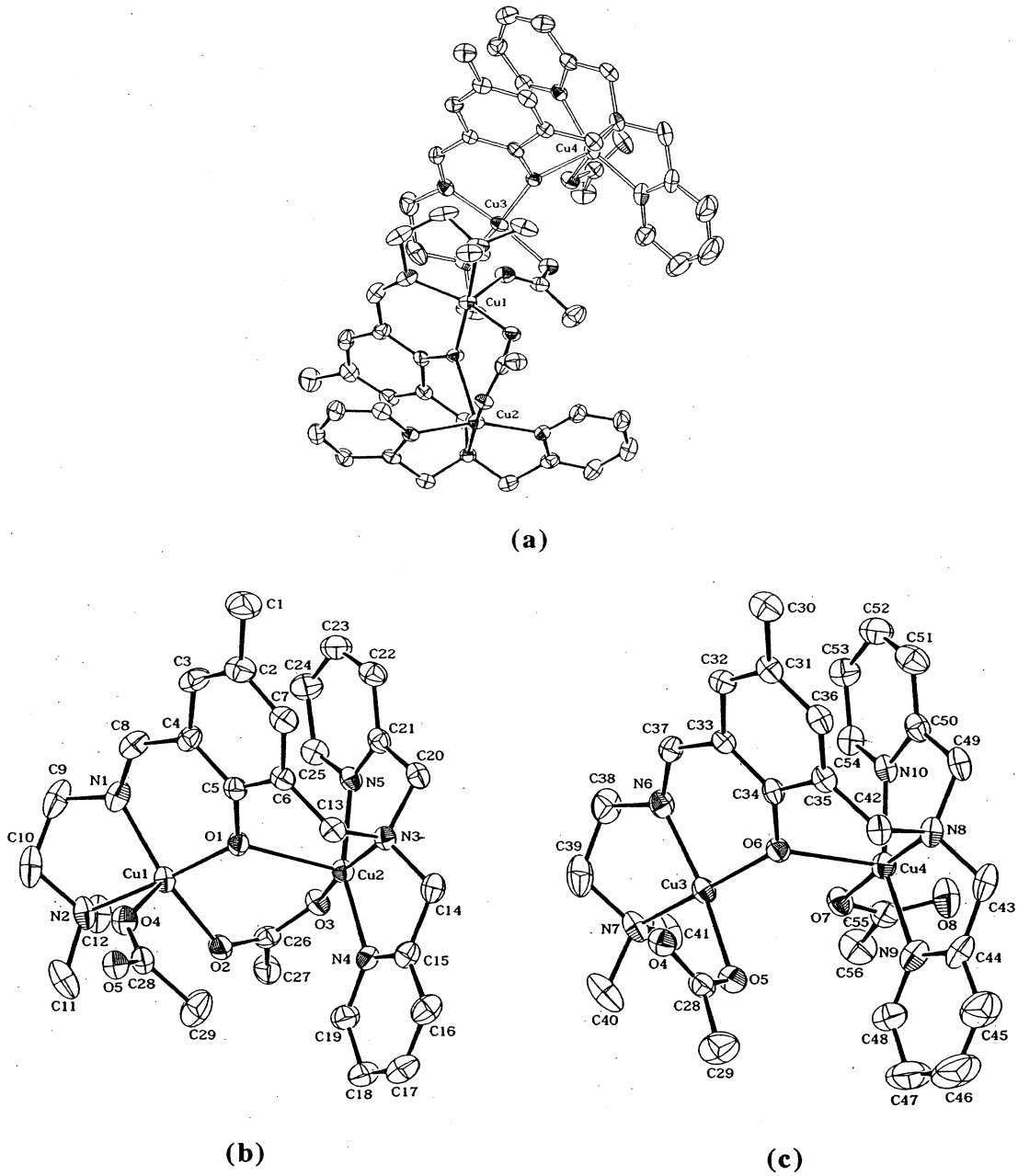

Figure 5. (a) An ORTEP view of $[Cu_4(L)_2(AcO)_3](ClO_4)_3 \cdot H_2O$ (**9**), (b) the structure of the dinuclear unit A with the atom numbering scheme, and (c) the structure of the unit B with the atom numbering scheme.

coordinate geometry for the M_b bound to the tridentate arm. A series of $Cu^{II}M^{II}$ complexes (**1**−**5**) have been derived because Cu^{II} prefers five-coordination to six-coordination. Another class isolated is the $Zn^{II}M^{II}$ complexes (M = Ni (**6**) and Co (**7**)) since Zn^{II} prefers five-coordination to a six-coordination compared with Co^{II} and Ni^{II} ions. However, six-coordinate Zn^{II} and five-coordinate Co^{II} and Ni^{II} are possible, and because of this **6** and **7** are more or less disproportionated in solution as evidenced by FAB mass spectrometry.

Visible Spectral Properties. Complexes **1**−**8** in DMF have a molar conductance of 60−74 S cm^2 mol^{-1} typical of 1:1 electrolytes in this solvent. In the case of $[CuNi(L)(AcO)(NCS)_2]$ (**8**), the NCS^- group weakly bonded to the Cu^{II} must be dissociated in DMF. Electronic absorption spectra of **1**−**8** in DMF are shown in Figures 6 and 7.

The electronic spectrum of **1** (CuMn) has an intense absorption band at 369 nm and a weak band at 631 nm (Figure 6). The former band is commonly observed for **1**−**8** and can be assigned to the $\pi-\pi^*$ transition associated with the azomethine linkage.[20,21] The latter is assigned to the d−d transition band of the Cu^{II} bound to the bidentate arm.[15] The other CuM complexes (**2**−**5**, **8**) show the Cu d−d band at a similar wavelength (610−650 nm). The d−d bands due to the Fe^{II} of **2** and the d−d bands due to the Co^{II} of **3** are not resolved in their spectra. The visible spectrum of **4** has a band near 950 nm that is attributable to a d−d component of the Ni^{II}. Complex **8** also shows a d−d band due to the Ni^{II} at 950 nm. The absorption spectra of **6** (insert in Figure

(20) Bosnich, B. *J. Am. Chem. Soc.* **1968**, *90*, 627.
(21) Downing, R. S.; Urbach, F. L. *J. Am. Chem. Soc.* **1969**, *91*, 5977.

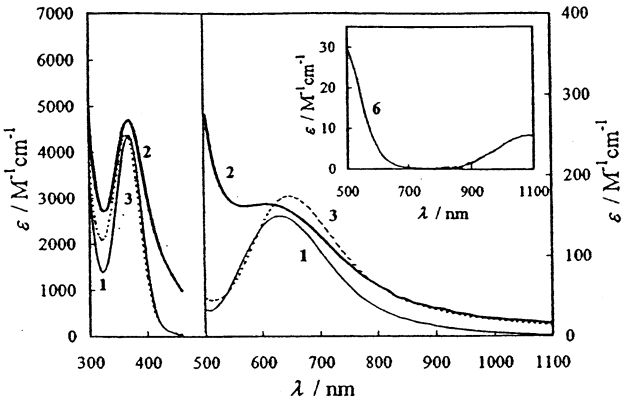

Figure 6. Electronic absorption spectra of $[CuMn(L)(AcO)_2]ClO_4$ (**1**), $[CuFe(L)(AcO)_2]ClO_4$ (**2**), and $[CuCo(L)(AcO)_2]ClO_4$ (**3**) in DMF. The insert is the visible spectrum of $[ZnCo(L)(AcO)_2]ClO_4$ (**6**).

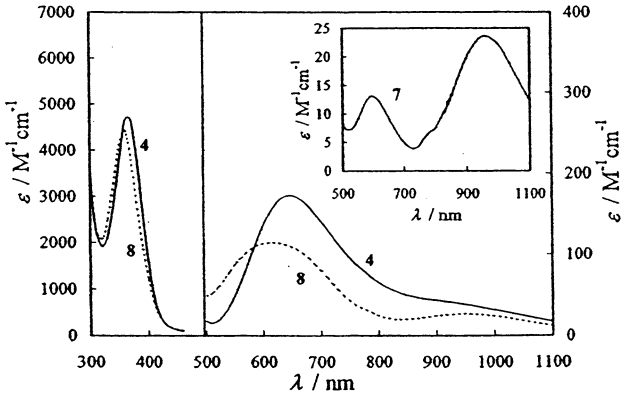

Figure 7. Electronic absorption spectra of $[CuNi(L)(AcO)_2]ClO_4$ (**4**) and $[CuNi(L)(AcO)(NCS)_2]$ (**8**) in DMF. The insert is the visible spectrum of $[ZnNi(L)(AcO)_2]ClO_4$ (**7**).

6) and **7** (insert in Figure 7) are typical of high-spin octahedral Co^{II} and Ni^{II}, respectively.

The electronic spectral results indicate that complexes **1**−**8** retain the heterodinuclear core in DMF although FAB mass spectrometric studies for **6** and **7** showed a partial disproportionation: $2Zn^{II}M^{II} \rightleftarrows Zn^{II}Zn^{II} + M^{II}M^{II}$ (M = Co, Ni).

The visible spectrum for a mixture of $[Cu_4(L)_2(AcO)_3](ClO_4)_3 \cdot H_2O$ (**9**) and $[Zn_2(L)(AcO)_2]ClO_4$ (1:2) in DMF is shown in Figure 8 together with the spectrum of $[CuZn(L)(AcO)_2]ClO_4$ (**5**) (trace a). The DMF solution of the mixture, soon after preparation, gave the spectrum of trace b that is exactly the spectrum of **9**. After the solution was warmed at 60 °C for 6 h, the spectrum of trace c was obtained, which is essentially the same as the spectrum of **5** (trace a). It is evident that $[CuZn(L)(AcO)_2]^+$ (**5**) is almost quantitatively

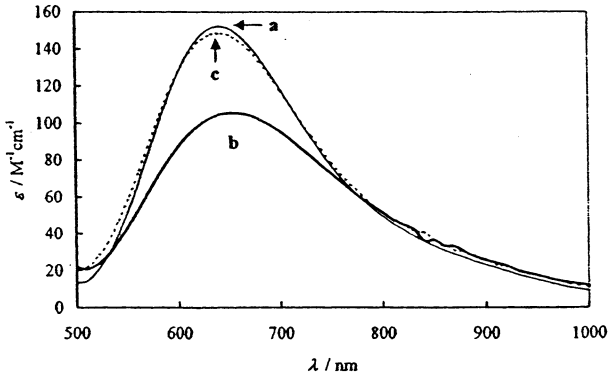

Figure 8. Visible spectra of $[CuZn(L)(AcO)_2]ClO_4$ (**5**) (a) and the 2:1 mixture of $[Zn_2(L)(AcO)_2]ClO_4$ and $[Cu_4(L)_2(AcO)_3](ClO_4)_3 \cdot H_2O$ (**9**) in DMF (b) soon after dissolution and (c) after being heated at 60 °C for 8 h.

formed in the solution based on the following equation; $(1/4)[Cu_4(L)_2(AcO)_3]^{3+} + (1/2)[Zn_2(L)(AcO)_2]^+ \rightarrow (7/8)[CuZn(L)(AcO)_2]^+ + (1/8)Cu^{II} + (1/8)Ni^{II} + (1/8)(L^-)$.

Conclusion

The unsymmetrical "end-off" compartmental ligand, 2-{*N*-[2-(dimethylamino)ethyl]iminomethyl}-6-[*N*,*N*-di(2-pyridylmethyl)aminomethyl]-4-methylphenol (HL), forms the discrete heterodinuclear complexes $[M_aM_b(L)(AcO)_2]ClO_4$ ($M_a = Cu^{II}$ and $M_b = Mn^{II}$, Fe^{II}, Co^{II}, Ni^{II}, Zn^{II}; $M_a = Zn^{II}$ and $M_b = Co^{II}$, Ni^{II}) and $[CuNi(L)(AcO)(NCS)_2]$ in a one-pot reaction. The site specificity of metal ions arises from the constraint of L^- providing a five-coordinate geometry for the M_a bound to the bidentate arm and a six-coordinate geometry for the M_b bound to the tridentate arm, along with exogenous acetate or the thiocyanate group. The complexes are stable to retain substantially the heterodinuclear core structure in solution.

Acknowledgment. This work was supported by a Grant-in-Aid for Scientific Research on Priority Area 'Metal-assembled Complexes (No. 10149106) and a Grant-in-Aid for COE Research 'Design and Control of Advanced Molecular Assembly System (No. 08CE2005) from the Ministry of Education, Science and Culture, Japan.

Supporting Information Available: Positional and thermal parameters of non-hydrogen atoms and full bond distances and angles for **1′**−**5′**, **6**, **7′**, **8′**, and **9** in CIF format. This material is available free of charge via the Internet at http://pubs.acs.org.

IC020002F